







PHOTONICS Research

Six-channel programmable coding metasurface simultaneously for orthogonal circular and linear polarizations

TONGHAO LIU,¹  YUEYU MENG,^{1,4}  JIAFU WANG,^{1,5} HUA MA,^{1,6} RUICHAO ZHU,¹  CHAO LIU,¹ WEIHAN LI,^{2,3} ZUNTIAN CHU,¹  SAI SUI,¹  TIANSHUO QIU,¹ WENXUAN TANG,^{2,3}  AND SHAOBO QU¹

¹Shaanxi Key Laboratory of Artificially-Structured Functional Materials and Devices, Air Force Engineering University, Xi'an 710051, China

²State Key Laboratory of Millimeter Waves, Southeast University, Nanjing 210096, China

³Frontiers Science Center for Mobile Information Communication and Security, Southeast University, Nanjing 210096, China

⁴e-mail: mengyy1990@163.com

⁵e-mail: wangjiafu1981@126.com

⁶e-mail: mahuar@xjtu.edu.cn

Received 20 January 2023; revised 25 April 2023; accepted 26 April 2023; posted 26 April 2023 (Doc. ID 486185); published 26 May 2023

Metasurfaces have intrigued long-standing research interests and developed multitudinous compelling applications owing to their unprecedented capability for manipulating electromagnetic waves, and the emerging programmable coding metasurfaces (PCMs) provide a real-time reconfigurable platform to dynamically implement customized functions. Nevertheless, most existing PCMs can only act on the single polarization state or perform in the limited polarization channel, which immensely restricts their practical application in multitask intelligent metadevices. Herein, an appealing strategy of the PCM is proposed to realize tunable functions in co-polarized reflection channels of orthogonal circularly polarized waves and in co-polarized and cross-polarized reflection channels of orthogonal linearly polarized waves from 9.0 to 10.5 GHz. In the above six channels, the spin-decoupled programmable meta-atom can achieve high-efficiency reflection and 1-bit digital phase modulation by selecting the specific ON/OFF states of two diodes, and the phase coding sequence of the PCM is dynamically regulated by the field-programmable gate array to generate the desired function. A proof-of-concept prototype is constructed to verify the feasibility of our methodology, and numerous simulation and experimental results are in excellent agreement with the theoretical predictions. This inspiring design opens a new avenue for constructing intelligent metasurfaces with higher serviceability and flexibility, and has tremendous application potential in communication, sensing, and other multifunctional smart metadevices. © 2023 Chinese Laser Press

<https://doi.org/10.1364/PRJ.486185>

1. INTRODUCTION

Metasurfaces, artificial planar arrangements of kaleidoscopic subwavelength meta-atoms, possess unparalleled ability to tailor the amplitude, phase, and polarization of electromagnetic (EM) waves [1–3]. Given the merits of small volume, low loss, simple fabrication, and exotic EM property, metasurfaces have evoked enormous interest and shown versatile applications ranging from the microwave to the visible domain, such as achromatic lenses, vortex beam generators, surface waves couplers, and meta-holograms [4–11]. More strikingly, a series of multifunctional metasurfaces with strong multiplexing capability are constructed to meet the application requirement of high integration. Some efforts are devoted to independently manipulating the wavefronts of orthogonal linearly polarized (LP) waves based on the metasurfaces with anisotropic structures [12,13]. And numerous schemes utilize chiral structures

or multiple phase modulations to completely decouple orthogonal circularly polarized (CP) waves and realize diverse functions [14–17]. In addition, certain multilayer metasurfaces composed of the structures with unequal dimensions can work at multiple frequency points for different incident waves [18–20]. But it is noteworthy that the above passive multifunctional metasurfaces are confined to fixed EM performance once fabricated, which inherently limits the flexibility of the metasurfaces in practical applications. Fortunately, the emergence of active metasurfaces effectively surmounts the aforementioned issue and makes numerous remarkable achievements.

By integrating the metasurfaces with active components controlled by electric bias, optical switch, mechanical actuation, and the like, active metasurfaces can dynamically control the characteristics of EM waves [21–24]. Among them, the metasurfaces loaded with positive-intrinsic-negative (PIN) diodes or

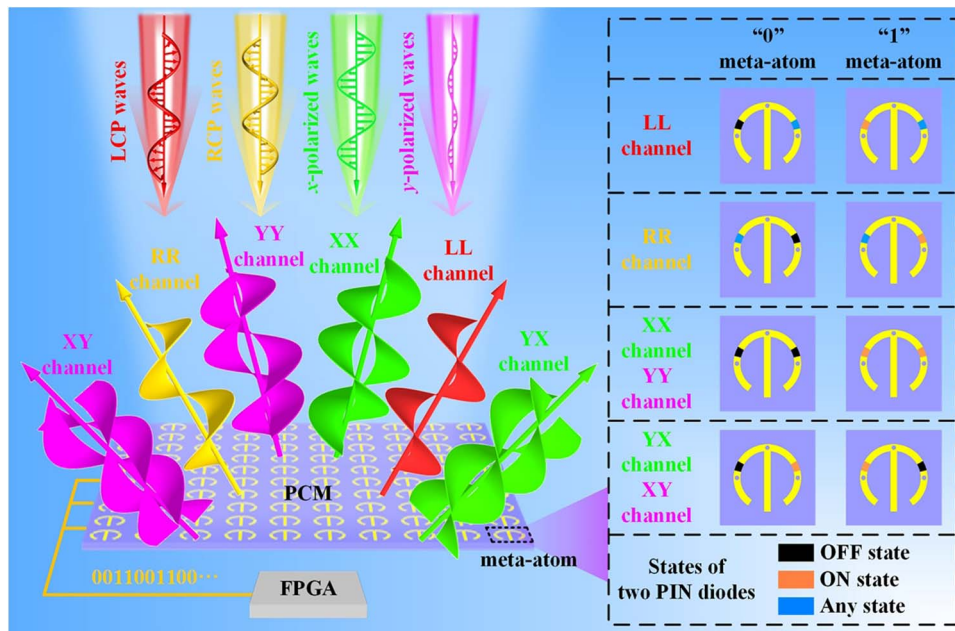


Fig. 1. Conceptual illustration of the proposed PCM, which can realize tunable functions for four polarization states and in six channels. The inset describes the mechanism that the spin-decoupled programmable meta-atom achieves 1-bit digital phase modulation in six channels. YX channel denotes the conversion from x -polarized incident waves to y -polarized reflected waves, and other channels can be interpreted similarly.

varactors driven by outer bias voltages are widely used at microwave frequencies due to the advantages of rapidity and simplicity [25,26]. In particular, the programmable coding metasurfaces (PCMs) have developed swiftly and constructed a bridge between the physical field and information science, in which the EM responses of meta-atoms are represented by the digital codes of “0” and “1” and the coding sequences of metasurfaces are dynamically regulated by the field-programmable gate array (FPGA) [27,28]. PCMs tremendously improve the design freedom of metasurfaces and make conspicuous progress in the application of smart metadevices. For instance, Li *et al.* reconstructed different holographic images with high resolution and low noise by the single PCM [29,30]. Wang *et al.* established the programmable polarization-modulated information metasurfaces based on the amplitude-phase-joint-coding technique to achieve encryption wireless communications [31,32]. Ma *et al.* combined the PCMs with intelligent sensing and control systems to fulfill self-adaptively programmable functions [33,34]. However, most existing PCMs are only applicable to incident waves of one or two polarization states to realize dynamically tunable functions, which restricts the application scenarios of the single PCM. Hence, the PCMs suitable for multiple polarization states are urgently needed to further improve the practicability and flexibility of the metasurfaces and satisfy the requirement of high-integration intelligent metadevices.

In this work, we propose an innovative paradigm of the PCM based on the spin-decoupled programmable meta-atom, which can dynamically and independently manipulate the wavefronts of orthogonal CP waves in co-polarized reflection channel and orthogonal LP waves in co-polarized and cross-polarized reflection channels from 9.0 to 10.5 GHz, as

illustrated in Fig. 1. Left-handed circularly polarized (LCP) waves and right-handed circularly polarized (RCP) waves are independently regulated by the left arm and the right arm of the umbrella-shaped structure of the meta-atom and can be reflected into co-polarized waves with high efficiency. Two identical PIN diodes are individually embedded into the left arm and the right arm, and the 1-bit co-polarized reflection phases of LCP waves and RCP waves are generated by switching the ON/OFF states of the left PIN diode and the right PIN diode, respectively. Based on the Jones matrix analysis, the meta-atom can realize efficient cross-polarized reflection for x -polarized waves and y -polarized waves when two PIN diodes are in the different states, and the 1-bit cross-polarized reflection phases can be generated by switching the states of two PIN diodes simultaneously. Furthermore, the meta-atom reflects x -polarized waves and y -polarized waves into co-polarized waves and possesses 1-bit co-polarized reflection phases when two PIN diodes are in two ON states and two OFF states. Consequently, the proposed PCM can accomplish tunable functions for four polarization states and in six channels by utilizing the FPGA to dynamically control the phase coding sequence of the PCM. Our methodology is strongly verified by abundant simulations and experiments and shows the unprecedented serviceability and design freedom for manipulating EM waves by metasurfaces.

2. META-ATOM DESIGN AND MECHANISM ANALYSIS

In order to construct a brand-new PCM that can act on multiple polarized incident waves, a spin-decoupled programmable meta-atom composed of three copper structure layers and two

F4B dielectric substrate layers ($\epsilon_r = 2.65$, $\tan \delta = 0.001$) is meticulously designed, as described in Fig. 2(a). Three copper structure layers comprise the top umbrella-shaped structure layer, the middle ground layer, and the bottom biasing layer, and the thickness of each copper structure layer is 0.017 mm. The symmetrical umbrella-shaped structure can be divided into the left arm, the right arm, and the middle handle. Two identical PIN diodes (SMP1320 from SKYWORKS) are loaded into the same position of two arms, and the equivalent circuits of the PIN diode under ON and OFF states are provided in Fig. 2(b). For the sake of simplifying the expression, the codes “00,” “01,” “10,” and “11” are used to denote four different states of two PIN diodes of the meta-atom, wherein, the “0” or “1” in the first bit of the four codes represents the OFF or ON state of the left PIN diode, and the “0” or “1” in the second bit represents the OFF or ON state of the right PIN diode. The middle handle is connected with the middle ground layer through a metallized via hole, and the other two metallized via holes penetrate from the left arm and the right arm to the biasing lines, respectively. Three copper structure layers are separated by two F4B dielectric substrate layers with the thicknesses of $d_1 = 4$ mm and $d_2 = 1$ mm.

The EM responses of the judiciously designed meta-atom are precisely simulated with the assistance of the computer simulation technology Microwave Studio. In the simulation, the meta-atom under different PIN diode states can achieve efficient co-polarized reflection for orthogonal CP incident waves at 10 GHz, and the induced surface current flows along the left arm under LCP incidence and flows along the right arm under RCP incidence, as depicted in Figs. 2(c)–2(f). Therefore, the co-polarized reflection phases of LCP waves and RCP waves can be independently modulated by adjusting the state of the left PIN diode and the right PIN diode, respectively. As displayed in Figs. 2(g) and 2(h), the simulated co-polarized reflection phase differences between the “00/01” meta-atoms and the “10/11” meta-atoms under LCP incidence are about π at 10 GHz, and the co-polarized reflection phase differences between the “00/10” meta-atoms and the “01/11” meta-atoms under RCP incidence are also about π , which means that the meta-atom can generate 1-bit co-polarized reflection phases for LCP waves and RCP waves by switching the ON/OFF states of the left PIN diode and the right PIN diode, respectively.

In addition, the EM responses of the meta-atom to LP incident waves are analyzed by the Jones matrix [35–37]. The

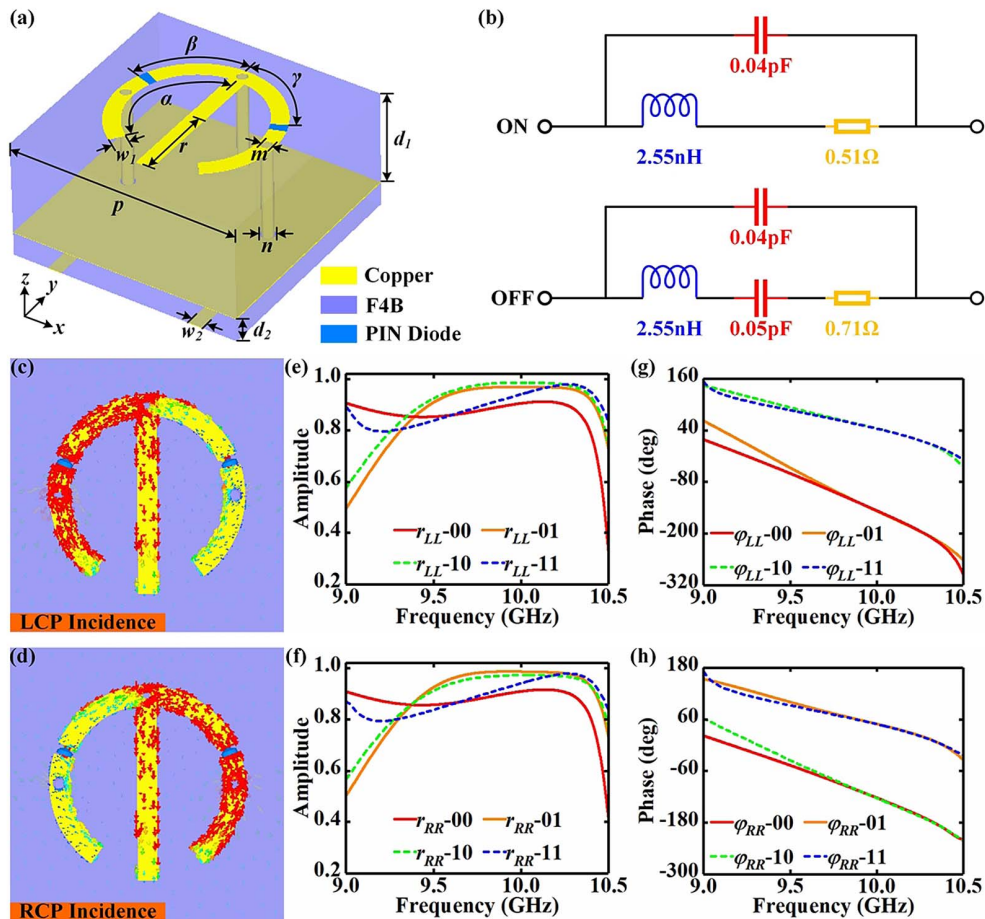


Fig. 2. (a) The schematic diagram of the spin-decoupled programmable meta-atom, where $p = 10$ mm, $d_1 = 4$ mm, $d_2 = 1$ mm, $w_1 = 0.7$ mm, $w_2 = 0.6$ mm, $\alpha = 145^\circ$, $\beta = 72^\circ$, $\gamma = 65^\circ$, $r = 3.5$ mm, $m = 0.5$ mm, and $n = 0.6$ mm. (b) The equivalent circuits of the PIN diode under ON and OFF states. (c), (d) Simulated surface current distributions of the spin-decoupled programmable meta-atom under orthogonal CP incidence. Simulated co-polarized reflection (e), (f) amplitudes and (g), (h) phases of the spin-decoupled programmable meta-atom with four different PIN diode states under orthogonal CP incidence.

relationship between LP incident waves and LP reflected waves can be written as follows:

$$\begin{pmatrix} E_x^r \\ E_y^r \end{pmatrix} = R_{LP} \cdot \begin{pmatrix} E_x^i \\ E_y^i \end{pmatrix} = \begin{pmatrix} R_{xx} & R_{xy} \\ R_{yx} & R_{yy} \end{pmatrix} \cdot \begin{pmatrix} E_x^i \\ E_y^i \end{pmatrix}. \quad (1)$$

Here, E_x^i and E_y^i denote x -polarized and y -polarized incident waves propagating along the $-z$ direction, and E_x^r and E_y^r denote x -polarized and y -polarized reflected waves propagating along the $+z$ direction. $R_{xx} = r_{xx} \cdot e^{i\varphi_{xx}}$ and $R_{yy} = r_{yy} \cdot e^{i\varphi_{yy}}$ are the co-polarized reflection coefficients under x -polarized and y -polarized incidence, where r_{xx} and r_{yy} represent the co-polarized reflection amplitudes, and φ_{xx} and φ_{yy} represent the co-polarized reflection phases. Similarly, $R_{yx} = r_{yx} \cdot e^{i\varphi_{yx}}$ and $R_{xy} = r_{xy} \cdot e^{i\varphi_{xy}}$ are the cross-polarized reflection coefficients under x -polarized and y -polarized incidence. On the basis of the previous simulation results, the cross-polarized reflection amplitudes of the proposed meta-atom under orthogonal CP illumination approach zero at 10 GHz, so the relationship between CP incident waves and CP reflected waves can be described as follows:

$$\begin{pmatrix} E_L^r \\ E_R^r \end{pmatrix} = R_{CP} \cdot \begin{pmatrix} E_L^i \\ E_R^i \end{pmatrix} = \begin{pmatrix} R_{LL} & 0 \\ 0 & R_{RR} \end{pmatrix} \cdot \begin{pmatrix} E_L^i \\ E_R^i \end{pmatrix}, \quad (2)$$

where E_L^i and E_R^i represent LCP and RCP incident waves propagating along the $-z$ direction, and E_L^r and E_R^r represent LCP and RCP reflected waves propagating along the $+z$ direction. $R_{LL} = r_{LL} \cdot e^{i\varphi_{LL}}$ and $R_{RR} = r_{RR} \cdot e^{i\varphi_{RR}}$ are the co-polarized reflection coefficients under LCP and RCP incidence. Moreover, CP incident waves and CP reflected waves can also be expressed by Eqs. (3) and (4) based on the relationship between LP waves and CP waves:

$$\begin{pmatrix} E_L^i \\ E_R^i \end{pmatrix} = \begin{pmatrix} 1 & -i \\ 1 & i \end{pmatrix} \cdot \begin{pmatrix} E_x^i \\ E_y^i \end{pmatrix} / \sqrt{2}, \quad (3)$$

$$\begin{pmatrix} E_L^r \\ E_R^r \end{pmatrix} = \begin{pmatrix} 1 & i \\ 1 & -i \end{pmatrix} \cdot \begin{pmatrix} E_x^r \\ E_y^r \end{pmatrix} / \sqrt{2}. \quad (4)$$

In the light of Eqs. (1)–(4), the relationship between the Jones matrix under CP basis R_{CP} and the Jones matrix under LP basis R_{LP} is derived as follows:

$$R_{LP} = \begin{pmatrix} 1 & i \\ 1 & -i \end{pmatrix}^{-1} \cdot R_{CP} \cdot \begin{pmatrix} 1 & -i \\ 1 & i \end{pmatrix}. \quad (5)$$

After calculation, Eq. (5) is further transformed into Eq. (6):

$$\begin{pmatrix} R_{xx} & R_{xy} \\ R_{yx} & R_{yy} \end{pmatrix} = \begin{pmatrix} r_{LL} \cdot e^{i\varphi_{LL}} + r_{RR} \cdot e^{i\varphi_{RR}} & -i(r_{LL} \cdot e^{i\varphi_{LL}} - r_{RR} \cdot e^{i\varphi_{RR}}) \\ -i(r_{LL} \cdot e^{i\varphi_{LL}} - r_{RR} \cdot e^{i\varphi_{RR}}) & -(r_{LL} \cdot e^{i\varphi_{LL}} + r_{RR} \cdot e^{i\varphi_{RR}}) \end{pmatrix} / 2. \quad (6)$$

The co-polarized reflection amplitudes r_{LL} and r_{RR} can be regarded as $r_{LL} \approx r_{RR} \approx 1$ at 10 GHz according to the simulation results in Figs. 2(e) and 2(f), and the difference between the co-polarized reflection phases φ_{LL} and φ_{RR} is defined as $\Delta\varphi = \varphi_{RR} - \varphi_{LL}$. Thus, Eq. (6) will be simplified as follows:

$$\begin{pmatrix} R_{xx} & R_{xy} \\ R_{yx} & R_{yy} \end{pmatrix} = \begin{pmatrix} (1 + e^{i\Delta\varphi})e^{i\varphi_{LL}} & (1 - e^{i\Delta\varphi})e^{i(\varphi_{LL}-\pi/2)} \\ (1 - e^{i\Delta\varphi})e^{i(\varphi_{LL}-\pi/2)} & (1 + e^{i\Delta\varphi})e^{i(\varphi_{LL}+\pi)} \end{pmatrix} / 2. \quad (7)$$

It can be found from Eq. (7) that $\begin{pmatrix} R_{xx} & R_{xy} \\ R_{yx} & R_{yy} \end{pmatrix} = \begin{pmatrix} e^{i\varphi_{LL}} & 0 \\ 0 & e^{i(\varphi_{LL}+\pi)} \end{pmatrix}$ when $\Delta\varphi = 0$ and $\begin{pmatrix} R_{xx} & R_{xy} \\ R_{yx} & R_{yy} \end{pmatrix} = \begin{pmatrix} 0 & e^{i(\varphi_{LL}-\pi/2)} \\ e^{i(\varphi_{LL}-\pi/2)} & 0 \end{pmatrix}$ when $\Delta\varphi = \pi$, which indicates that the meta-atom will efficiently reflect x -polarized and y -polarized waves into co-polarized waves by keeping the ON/OFF states of the left PIN diode and the right PIN diode identical, and will reflect x -polarized and y -polarized waves into cross-polarized waves by making the ON/OFF states of two PIN diodes different. More importantly, 1-bit co-polarized reflection phases are generated when two PIN diodes with the same ON/OFF states are switched simultaneously, and 1-bit cross-polarized reflection phases are generated when two PIN diodes with diverse ON/OFF states are switched simultaneously. The simulation results in Figs. 3(a) and 3(b) show that the “00” meta-atom and “11” meta-atom have extremely high co-polarized reflection amplitudes under x -polarized and y -polarized incidence at 10 GHz, and the “01” meta-atom and “10” meta-atom possess high cross-polarized reflection amplitudes. In addition, the co-polarized reflection phase differences between the “00” meta-atom and “11” meta-atom under x -polarized and y -polarized incidence are around π at 10 GHz, and the cross-polarized reflection phase differences between the “01” meta-atom and “10” meta-atom are also around π , as presented in Figs. 3(c) and 3(d). To sum up, the simulation results effectively confirm the previous theoretical analysis, and suggest that the established spin-decoupled programmable meta-atom is able to efficiently realize 1-bit dig-

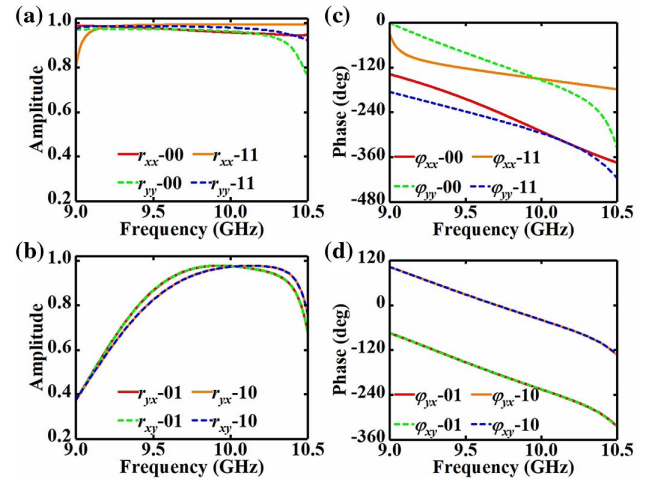


Fig. 3. Simulated co-polarized and cross-polarized reflection (a), (b) amplitudes and (c), (d) phases of the spin-decoupled programmable meta-atom with four different PIN diode states under x -polarized and y -polarized incidence.

ital phase modulation in two CP channels and four LP channels.

3. DESIGN AND SIMULATION OF THE PCM

According to the aforementioned design and analysis of the proposed spin-decoupled programmable meta-atom, a PCM composed of 30×30 meta-atoms is constructed to perform tunable functions in six channels, whose phase coding sequence can be dynamically adjusted by the FPGA. Two groups of schemes (Scheme A and Scheme B) are provided to demonstrate our methodology. In Scheme A, the PCM is designed to generate dual-beam patterns with distinct deflection angles in different channels. The phase distributions of the PCM in six channels are displayed in Figs. 4(a)–4(f), where the reflection phases of 0 and π can be represented by the codes “0” and “1,” respectively. In the light of the generalized Snell’s law [1,38,39], the deflection angle θ of two scattering beams can be calculated as follows:

$$k_0 \sin \theta = k_0 \sin \theta_i + d\varphi/dx, \tag{8}$$

where k_0 denotes the wavenumber of EM waves in free space, dx is the period of a group of meta-atoms with the same reflection phase, the phase difference between two adjacent groups of meta-atoms is $d\varphi = \pi$ in this 1-bit PCM, and the incident angle is $\theta_i = 0$ when the incident waves normally illuminate onto the PCM. On the basis of Figs. 4(a)–4(f) and Eq. (8), the theoretical deflection angles of the desired dual-beam patterns in the *LL* channel, *RR* channel, *XX* channel, *YY* channel, *YX* channel, and *XY* channel at 10 GHz are $\pm 48.6^\circ$, $\pm 30.0^\circ$, $\pm 22.0^\circ$, $\pm 17.5^\circ$, $\pm 14.5^\circ$, and $\pm 12.4^\circ$, respectively. The far-field simulation results exhibited in Fig. 5 indicate that two obvious scattering beams are produced by the PCM in six channels, and the simulated deflection angles of the generated beams are in excellent accordance with the theoretical results. Significantly, the broadband performances of the PCM in six channels are evaluated. As portrayed in Fig. 6, the simulated deflection angle distributions of the

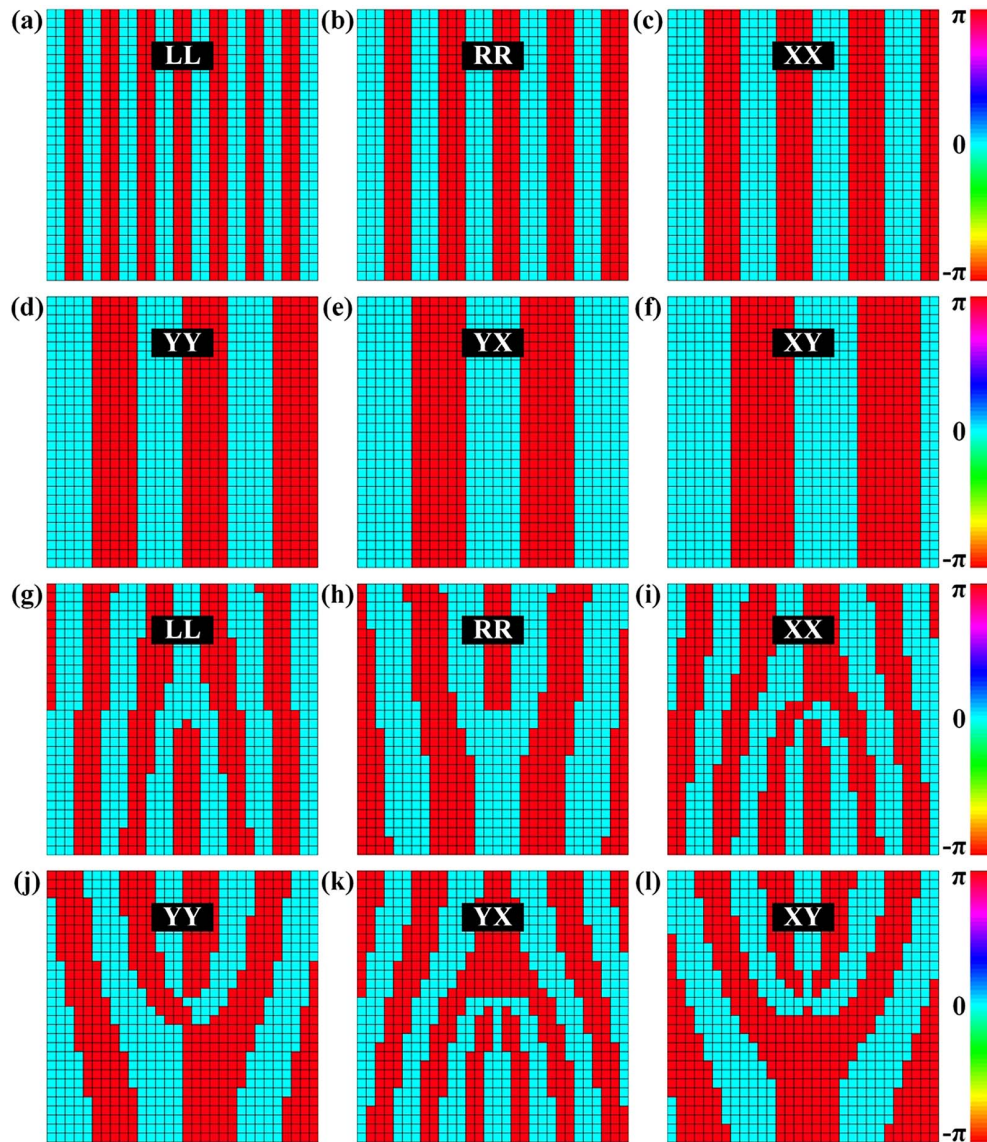


Fig. 4. Phase distributions of the PCM in six channels in (a)–(f) Scheme A and (g)–(l) Scheme B.

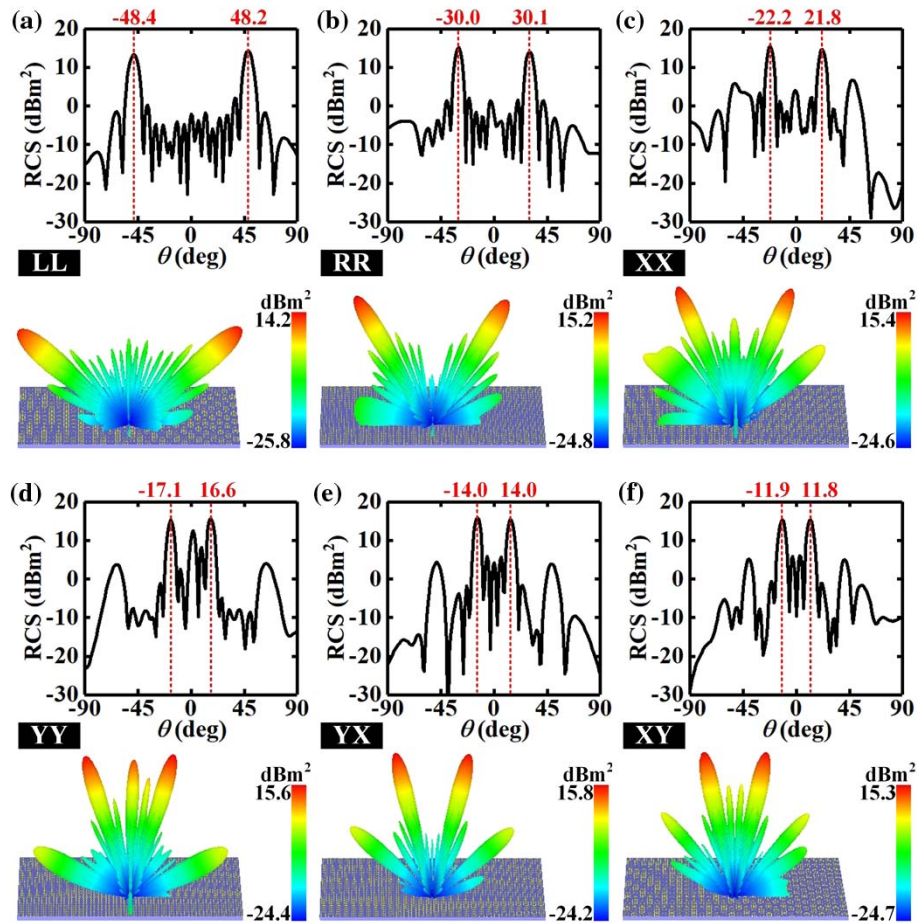


Fig. 5. Simulated bistatic RCS curves (top panels) and 3D far-field scattering patterns (bottom panels) of Scheme A in (a) *LL* channel, (b) *RR* channel, (c) *XX* channel, (d) *YY* channel, (e) *YX* channel, and (f) *XY* channel at 10 GHz.

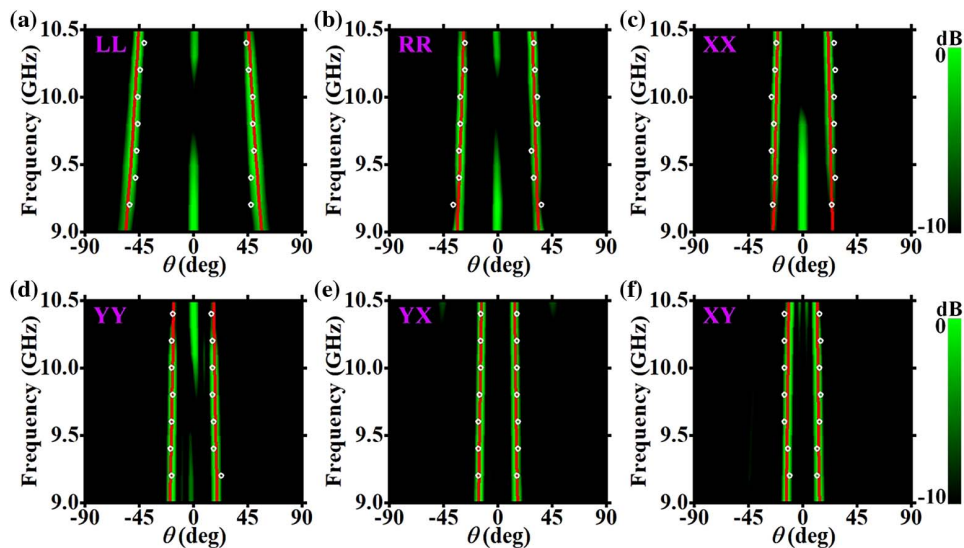


Fig. 6. Simulated normalized scattering field distributions of Scheme A in (a) *LL* channel, (b) *RR* channel, (c) *XX* channel, (d) *YY* channel, (e) *YX* channel, and (f) *XY* channel from 9.0 to 10.5 GHz. The theoretical results and experimental results are represented by red lines and white circles, respectively.

normalized scattering fields in six channels almost agree with the theoretical results (red lines) calculated by Eq. (8) at 9.0–10.5 GHz, which suggests that the proposed PCM possesses the wide working bandwidth from 9.0 to 10.5 GHz in six channels. The slight deflection angle deviation of the scattering beams and the relatively large energy of the specular reflection mainly result from the imperfect 1-bit reflection phases of the meta-atom and the discrete phase distributions of the PCM.

Additionally, Scheme B is presented to utilize the PCM to generate vortex beams with different topological charge l and deflection angle θ in six channels. The required phase distribution $\varphi(x, y)$ for vortex beam generation can be described as follows [40–42]:

$$\varphi(x, y) = l \cdot \arctan(y/x) + k_0 \cdot x \cdot \sin \theta, \quad (9)$$

where (x, y) is the established 2D coordinate. Due to the 1-bit digital phase modulation of the proposed PCM, the phase distribution $\varphi(x, y)$ needs to be discretized based on Eq. (10):

$$\varphi(x, y) = \begin{cases} 0, & 0 \leq \varphi(x, y) < \pi \\ \pi, & \pi \leq \varphi(x, y) < 2\pi \end{cases} \quad (10)$$

In our design, the topological charges of the produced vortex beams propagating in the $-x$ direction in the *LL* channel, *RR* channel, *XX* channel, *YY* channel, *YX* channel, and *XY* channel are +1, -1, +2, -2, +3, and -3, respectively, and the vortex beams propagating in the $+x$ direction in these six channels possess the topological charges of -1, +1, -2, +2, -3, and +3, respectively. Furthermore, the deflection angles of two vortex beams in the *LL* channel, *RR* channel, *XX* channel, *YY* channel, *YX* channel, and *XY* channel are $\pm 30^\circ$, $\pm 20^\circ$, $\pm 30^\circ$, $\pm 20^\circ$, $\pm 30^\circ$, and $\pm 20^\circ$ at 10 GHz. Thereupon, the

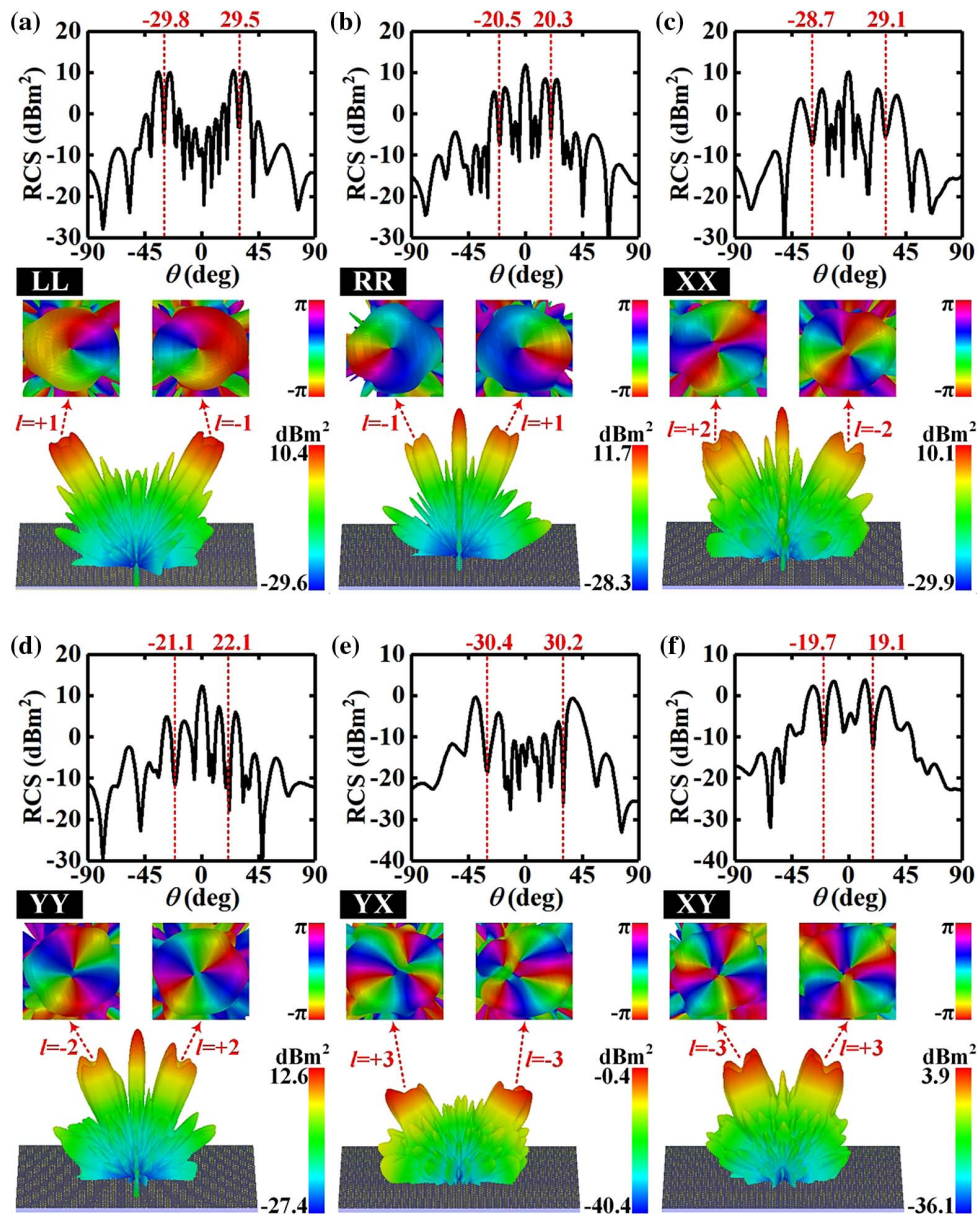


Fig. 7. Simulated bistatic RCS curves (top panels), phase profiles of the scattering beams (middle panels), and 3D far-field scattering patterns (bottom panels) of Scheme B in (a) *LL* channel, (b) *RR* channel, (c) *XX* channel, (d) *YY* channel, (e) *YX* channel, and (f) *XY* channel at 10 GHz.

phase distributions of the PCM in six channels are calculated by Eqs. (9) and (10) and provided in Figs. 4(g)–4(l). It can be observed from the far-field simulation results in Fig. 7 that the two beams generated in each channel exhibit the ring-shaped intensity profile with the hollow center, and the energy null of each beam is nearly located at the pre-designed beam deflection angle, which are in line with the characteristics of the vortex beam. Moreover, the phase profiles of the beams indicate that two vortex beams with desired topological charges are generated by the PCM in each channel. In summary, the aforementioned two groups of simulation schemes demonstrate that our proposed PCM is able to realize tunable functions in six channels.

4. EXPERIMENTAL SECTION

As presented in Fig. 8(a), an elaborate prototype identical to the simulation model is fabricated with low-cost printed circuit board (PCB) technology to further validate the practicability of our designed PCM, in which the required PIN diodes are welded at the corresponding positions of the prototype. The far-field experiments of the prototype are implemented in the microwave anechoic chamber, and the experimental setups consist of the vector network analyzer (VNA), the CP horn antennas, the LP horn antennas, the FPGA, and the turntable mount, as exhibited in Fig. 8(b). In order to measure the

far-field scattering patterns of the prototype under normal illumination of CP and LP waves, the prototype and the transmitting horn antenna connected to port 1 of the VNA are fixed on the turntable mount, and the receiving horn antenna connected to port 2 of the VNA is placed far enough from the prototype, which ensure that the transmitting horn antenna is always set along the normal of the prototype and the receiving horn antenna can rotate around the prototype. The coding sequences of the six channels in the experiment are the same as those of Scheme A in the simulation, which are dynamically controlled by the connected FPGA. The measured normalized far-field scattering patterns in Figs. 8(c)–8(h) reveal that the scattering beams with the deflection angles close to the theoretical values are generated in six channels at 10 GHz, and the discrepancy of deflection angles between theoretical and experimental results does not exceed 4° . In addition, the broadband performances of the prototype in six channels are measured and provided in Fig. 6, which are essentially consistent with the theoretical results and simulation results. The deviation of the experimental results is mainly due to the imperfect placement of the experimental setup, inaccurate performance of the PIN diodes, and the inevitable fabrication errors in PCB processing and PIN diodes welding. But overall, the experimental results agree with the theoretical predictions, and strongly prove the availability of our proposed PCM.

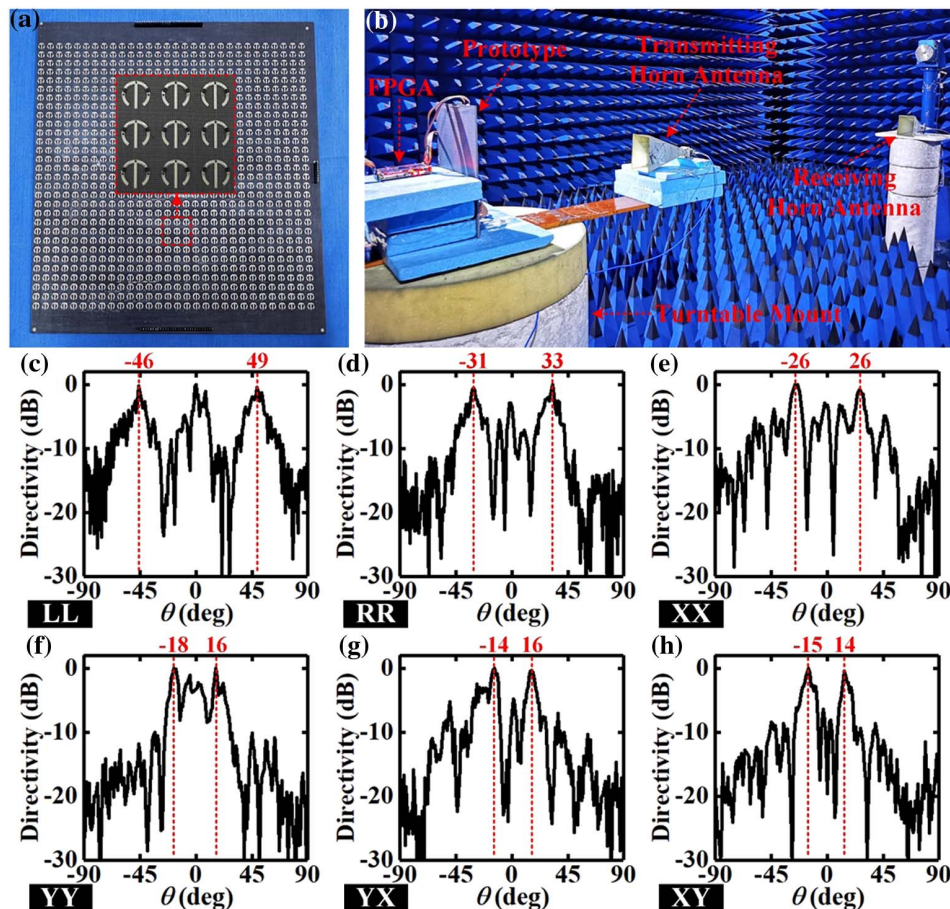


Fig. 8. (a) Fabricated prototype of the proposed PCM. (b) Far-field experimental setup. The measured normalized far-field scattering patterns in (c) LL channel, (d) RR channel, (e) XX channel, (f) YY channel, (g) YX channel, and (h) XY channel at 10 GHz.

5. CONCLUSION

In this paper, we construct an ingenious PCM to achieve tunable functions for four polarization states and in six channels from 9.0 to 10.5 GHz. By switching the two PIN diodes of the spin-decoupled programmable meta-atom to the specific ON/OFF states, the meta-atom can reflect LCP waves and RCP waves into corresponding co-polarized waves, and can reflect x -polarized waves and y -polarized waves into co-polarized waves and cross-polarized waves. In addition, the meta-atom is able to realize 1-bit digital phase modulation in the above six channels, which enables the established PCM to dynamically generate arbitrary desired functions by using the FPGA to control its phase coding sequence. A series of simulations and experiments collectively corroborate the availability of our proposed PCM. Compared with most existing paradigms, our simple design further improves the serviceability and flexibility of the PCM, and has promising application prospects in encrypted communication, self-adaptive imaging, and other high-integration intelligent metadevices. More importantly, this generic design framework of the PCM can achieve multibit phase modulation and complex amplitude modulation to efficiently complete more sophisticated functions after introducing varactors and varistor diodes, respectively, and may be extended to other frequency domains by replacing PIN diodes with other appropriate phase changing materials such as $\text{Ge}_2\text{Sb}_2\text{Te}_5$ and vanadium dioxide.

Funding. Air Force Engineering University (KGD080921020); Natural Science Basic Research Program of Shaanxi Province (2021JQ-363); Fundamental Research Funds for the Central Universities (2242022k30004); National Natural Science Foundation of China (61901508, 61971435, 62101589, 62201609).

Disclosures. The authors declare no conflicts of interest.

Data Availability. Data underlying the results presented in this paper are not publicly available at this time but may be obtained from the authors upon reasonable request.

REFERENCES

- N. Yu, P. Genevet, M. Kats, F. Aieta, J. P. Tetienne, F. Capasso, and Z. Gaburro, "Light propagation with phase discontinuities: generalized laws of reflection and refraction," *Science* **334**, 333–337 (2011).
- C. Pfeiffer and A. Grbic, "Metamaterial Huygens' surfaces: tailoring wave fronts with reflectionless sheets," *Phys. Rev. Lett.* **110**, 197401 (2013).
- X. G. Luo, "Principles of electromagnetic waves in metasurfaces," *Sci. China Phys. Mech. Astron.* **58**, 594201 (2015).
- S. Wang, P. C. Wu, V. C. Su, Y. C. Lai, C. Hung Chu, J. W. Chen, S. H. Lu, J. Chen, B. Xu, C. H. Kuan, T. Li, S. Zhu, and D. P. Tsai, "Broadband achromatic optical metasurface devices," *Nat. Commun.* **8**, 187 (2017).
- K. Zhang, Y. Yuan, X. Ding, H. Li, B. Ratni, Q. Wu, J. Liu, S. N. Burokur, and J. Tan, "Polarization-engineered noninterleaved metasurface for integer and fractional orbital angular momentum multiplexing," *Laser Photonics Rev.* **15**, 2000351 (2021).
- H. X. Xu, H. Liu, X. Ling, Y. Sun, and F. Yuan, "Broadband vortex beam generation using multimode Pancharatnam-Berry metasurface," *IEEE Trans. Antennas Propag.* **65**, 7378–7382 (2017).
- W. Sun, Q. He, S. Sun, and L. Zhou, "High-efficiency surface plasmon meta-couplers: concept and microwave-regime realizations," *Light Sci. Appl.* **5**, e16003 (2016).
- Z. Wang, S. Li, X. Zhang, X. Feng, Q. Wang, J. Han, Q. He, W. Zhang, S. Sun, and L. Zhou, "Excite spoof surface plasmons with tailored wavefronts using high-efficiency terahertz metasurfaces," *Adv. Sci.* **7**, 2000982 (2020).
- L. Huang, S. Zhang, and T. Zentgraf, "Metasurface holography: from fundamentals to applications," *Nanophotonics* **7**, 1169–1190 (2018).
- W. Li, Q. Ma, C. Liu, Y. Zhang, X. Fu, J. Wang, S. Gao, T. Qiu, T. Liu, Q. Xiao, J. Wei, T. Gu, Z. Zhou, F. Li, Q. Cheng, L. Li, W. Tang, and T. Cui, "Intelligent metasurface system for automatic tracking of moving targets and wireless communications based on computer vision," *Nat. Commun.* **14**, 989 (2023).
- Z. Zhen, C. Qian, Y. Jia, Z. Fan, R. Hao, T. Cai, B. Zheng, H. Chen, and E. Li, "Realizing transmitted metasurface cloak by a tandem neural network," *Photonics Res.* **9**, B229–B235 (2021).
- H. F. Ma, Y. Q. Liu, K. Luan, and T. J. Cui, "Multi-beam reflections with flexible control of polarizations by using anisotropic metasurfaces," *Sci. Rep.* **6**, 39390 (2016).
- Y. Jing, Y. Li, J. Zhang, J. Wang, M. Feng, H. Ma, and S. Qu, "Full-space-manipulated multifunctional coding metasurface based on "Fabry-Pérot-like" cavity," *Opt. Express* **27**, 21520–21531 (2019).
- T. Liu, X. Fu, J. Wang, Y. Meng, H. Ma, X. Li, R. Zhu, X. Wang, W. Li, W. Tang, Y. Li, and S. Qu, "Single-layer achiral metasurface with independent amplitude–phase control for both left-handed and right-handed circular polarizations," *ACS Appl. Mater. Interfaces* **14**, 33968–33975 (2022).
- H. X. Xu, L. Han, Y. Li, Y. Sun, J. Zhao, S. Zhang, and C. W. Qiu, "Completely spin-decoupled dual-phase hybrid metasurfaces for arbitrary wavefront control," *ACS Photonics* **6**, 211–220 (2018).
- Y. Yuan, K. Zhang, B. Ratni, Q. Song, X. Ding, Q. Wu, S. N. Burokur, and P. Genevet, "Independent phase modulation for quadruplex polarization channels enabled by chirality-assisted geometric-phase metasurfaces," *Nat. Commun.* **11**, 4186 (2020).
- H. Hou, G. Wang, H. Li, W. Guo, and T. Cai, "Helicity-dependent metasurfaces employing receiver-transmitter meta-atoms for full-space wavefront manipulation," *Opt. Express* **28**, 27575–27587 (2020).
- H. Xu, G. Hu, M. Jiang, S. Tang, Y. Wang, C. Wang, Y. Huang, X. Ling, H. Liu, and J. Zhou, "Wavevector and frequency multiplexing performed by a spin-decoupled multichannel metasurface," *Adv. Mater. Technol.* **5**, 1900710 (2020).
- T. Liu, W. Li, Y. Meng, W. Tang, H. Ma, X. Li, R. Zhu, C. Liu, H. Zhang, J. Wang, and S. Qu, "High-fidelity multiplexing meta-hologram for information display, storage and encryption," *Mater. Des.* **224**, 111353 (2022).
- Q. Fang, L. Wu, W. Pan, M. Li, and J. Dong, "Trifunctional metasurface for manipulating linearly and circularly polarized waves in transmission and reflection modes," *Appl. Phys. Lett.* **117**, 074102 (2020).
- A. Nemati, Q. Wang, N. S. S. Ang, W. Wang, M. Hong, and J. Teng, "Ultra-high extinction-ratio light modulation by electrically tunable metasurface using dual epsilon-near-zero resonances," *Opto-Electron. Adv.* **4**, 200088 (2021).
- Y. H. Fu, A. Q. Liu, W. M. Zhu, X. M. Zhang, D. P. Tsai, J. B. Zhang, T. Mei, J. F. Tao, H. C. Guo, X. H. Zhang, J. H. Teng, N. I. Zheludev, G. Q. Lo, and D. L. Kwong, "A micromachined reconfigurable metamaterial via reconfiguration of asymmetric split-ring resonators," *Adv. Funct. Mater.* **21**, 3589–3594 (2011).
- M. X. Ren, W. Wu, W. Cai, B. Pi, X. Z. Zhang, and J. J. Xu, "Reconfigurable metasurfaces that enable light polarization control by light," *Light Sci. Appl.* **6**, e16254 (2017).
- L. Chen, Q. Ma, Q. F. Nie, Q. R. Hong, H. Y. Cui, Y. Ruan, and T. J. Cui, "Dual-polarization programmable metasurface modulator for near-field information encoding and transmission," *Photonics Res.* **9**, 116–124 (2021).
- X. L. Ma, W. B. Pan, C. Huang, M. B. Pu, Y. Q. Wang, B. Zhao, J. H. Cui, C. T. Wang, and X. G. Luo, "An active metamaterial for polarization manipulating," *Adv. Opt. Mater.* **2**, 945–949 (2014).
- R. Zhu, J. Wang, T. Qiu, Y. Han, X. Fu, Y. Shi, X. Liu, T. Liu, Z. Zhang, Z. Chu, C. Qiu, and S. Qu, "Remotely mind-controlled metasurface via brainwaves," *eLight* **2**, 10 (2022).

27. T. J. Cui, M. Q. Qi, X. Wan, J. Zhao, and Q. Cheng, "Coding metamaterials, digital metamaterials and programmable metamaterials," *Light Sci. Appl.* **3**, e218 (2014).
28. Q. Ma and T. J. Cui, "Information metamaterials: bridging the physical world and digital world," *Photonix* **1**, 1 (2020).
29. L. Li, T. J. Cui, W. Ji, S. Liu, J. Ding, X. Wan, Y. Bo Li, M. Jiang, C. W. Qiu, and S. Zhang, "Electromagnetic reprogrammable coding-metasurface holograms," *Nat. Commun.* **8**, 197 (2017).
30. L. Li, H. Ruan, C. Liu, Y. Li, Y. Shuang, A. Alù, C. W. Qiu, and T. J. Cui, "Machine-learning reprogrammable metasurface imager," *Nat. Commun.* **10**, 1082 (2019).
31. H. L. Wang, H. F. Ma, and T. J. Cui, "A polarization-modulated information metasurface for encryption wireless communications," *Adv. Sci.* **9**, 2204333 (2022).
32. C. X. Huang, J. Zhang, Q. Cheng, and T. J. Cui, "Polarization modulation for wireless communications based on metasurfaces," *Adv. Funct. Mater.* **31**, 2103379 (2021).
33. Q. Ma, Q. R. Hong, X. X. Gao, H. B. Jing, C. Liu, G. D. Bai, Q. Cheng, and T. J. Cui, "Smart sensing metasurface with self-defined functions in dual polarizations," *Nanophotonics* **9**, 3271–3278 (2020).
34. Q. Ma, G. D. Bai, H. B. Jing, C. Yang, L. Li, and T. J. Cui, "Smart metasurface with self-adaptively reprogrammable functions," *Light Sci. Appl.* **8**, 98 (2019).
35. R. Jones, "A new calculus for the treatment of optical systems I. Description and discussion of the calculus," *J. Opt. Soc. Am.* **31**, 488–493 (1941).
36. C. Menzel, C. Rockstuhl, and F. Lederer, "Advanced Jones calculus for the classification of periodic metamaterials," *Phys. Rev. A* **82**, 053811 (2010).
37. Q. Hu, K. Chen, J. Zhao, S. Dong, T. Jiang, and Y. Feng, "On-demand dynamic polarization meta-transformer," *Laser Photonics Rev.* **17**, 2200479 (2023).
38. F. Aieta, P. Genevet, N. Yu, M. A. Kats, Z. Gaburro, and F. Capasso, "Out-of-plane reflection and refraction of light by anisotropic optical antenna metasurfaces with phase discontinuities," *Nano Lett.* **12**, 1702–1706 (2012).
39. A. Díaz-Rubio, V. S. Asadchy, A. Elsakka, and S. A. Tretyakov, "From the generalized reflection law to the realization of perfect anomalous reflectors," *Sci. Adv.* **3**, e1602714 (2017).
40. Z. Zhang, J. Wang, R. Zhu, Y. Jia, T. Liu, M. Yan, J. Jiang, Y. Li, Y. Meng, and S. Qu, "Multifunctional full-space metasurface controlled by frequency, polarization and incidence angle," *Opt. Express* **29**, 7544–7557 (2021).
41. T. Liu, W. Li, Y. Meng, H. Ma, W. Tang, G. Li, H. Shi, S. Sui, J. Wang, and S. Qu, "Six-mode orbital angular momentum generator enabled by helicity-assisted full-space metasurface with flexible manipulation of phase, polarization, and spatial information," *Adv. Opt. Mater.* **10**, 2102638 (2022).
42. D. Zhang, X. Cao, H. Yang, J. Gao, and X. Zhu, "Multiple OAM vortex beams generation using 1-bit metasurface," *Opt. Express* **26**, 24804–24815 (2018).